Available online at www.sciencedirect.com

ScienceDirect

Publishing Services by Elsevier

International Journal of Naval Architecture and Ocean Engineering 10 (2018) 282–293
http://www.journals.elsevier.com/international-journal-of-naval-architecture-and-ocean-engineering/

Three-dimensional trajectory tracking for underactuated AUVs with bio-inspired velocity regulation

Jiajia Zhou [a], Dingqi Ye [a], Junpeng Zhao [b], Dongxu He [a,*]

[a] *Harbin Engineering University, Harbin 150001, China*
[b] *Beijing Institute of Aerospace Control Devices, Beijing 100039, China*

Received 4 October 2016; revised 13 June 2017; accepted 19 August 2017
Available online 21 October 2017

Abstract

This paper attempts to address the motion parameter skip problem associated with three-dimensional trajectory tracking of an underactuated Autonomous Underwater Vehicle (AUV) using backstepping-based control, due to the unsmoothness of tracking trajectory. Through kinematics concepts, a three-dimensional dynamic velocity regulation controller is derived. This controller makes use of the surge and angular velocity errors with bio-inspired models and backstepping techniques. It overcomes the frequently occurring problem of parameter skip at inflection point existing in backstepping tracking control method and increases system robustness. Moreover, the proposed method can effectively avoid the singularity problem in backstepping control of virtual velocity error. The control system is proved to be uniformly ultimately bounded using Lyapunov stability theory. Simulation results illustrate the effectiveness and efficiency of the developed controller, which can realize accurate three-dimensional trajectory tracking for an underactuated AUV with constant external disturbances.

Keywords: Dynamic velocity regulation; Bio-inspired model; Backstepping; Underactuated AUV; Three-dimensional trajectory tracking

1. Introduction

Precise three-dimensional trajectory tracking of Autonomous Underwater Vehicles (AUVs) is an important technical prerequisite for marine resources development, scientific investigation, and offshore defense (Thor I. Fossen, 2011; Do Wan Kim, 2015; Yu-shan Sun et al., 2016). However, unmanned AUVs are usually underactuated, highly coupled, and nonlinear (K.D. Do, 2015; Fossen. T. I et al., 2015). The AUV studied in this paper lacks actuators in the sway and heave directions, and thus can be classified as a typical underactuated system. With external disturbances, as well as time and space requirements, three-dimensional trajectory tracking of AUV is further complicated.

Currently, several methods have been proposed to track underactuated AUVs, such as sliding mode control (Taha Elmokadem et al., 2016; Zheping Yan et al., 2015; Jia He-ming et al., 2012a,b), neural network control (Zhou et al., 2013), and backstepping technique (F.Y. Bi et al., 2010; Jia He-ming et al., 2012a,b; Wang Hong-Jian et al., 2015; Aguiar, A. and Joao, P. 2007; Xu et al., 2014). These control methods have their own advantages and limitations. Taha Elmokadem et al. (2016) combined a hyperbolic function with sliding mode control, based on which the speed jump problem was solved and planar trajectory tracking for an underactuated AUV was achieved. In order to deal with the disturbances caused by model parameters and unknown external environment, Zheping Yan et al. (2015) proposed a method to realize global finite-time planar trajectory tracking for an underactuated vehicle. These two methods above are still limited to control only in the horizontal plane, without taking account of three-dimensional trajectory tracking. To achieve three-dimensional trajectory tracking control, Jia He-ming et al.

* Corresponding author.
E-mail address: hedongxu_heu@163.com (D. He).
Peer review under responsibility of Society of Naval Architects of Korea.

https://doi.org/10.1016/j.ijnaoe.2017.08.006

(2012a,b) used a nonlinear iteration-based sliding mode to lower the chattering of the hydroplane and reduce the overshoot. However, these methods still have difficulties in fundamentally solving the issue of chatting associated with sliding mode control. Zhou, Jiajia et al. (2013) proposed three neural network controllers to estimate unknown parameters and external disturbances, where a desired spatial path was tracked successfully for an AUV. However, learning of the neural network was indeed time consuming.

In order to tackle the speed jump problem of backstepping technique, F.Y. Bi et al. (2010) simplified the mid-calculation process in traditional backstepping method using virtual velocity errors, making AUV tracking control possible in a horizontal plane. Jia He-ming et al. (2012a,b) proposed an adaptive backstepping approach to suppress disturbances from ocean current and achieved three-dimensional path tracking control. Wang Hong-Jian et al. (2015) developed a filtered backstepping method to simplify the process of obtaining derivatives and filter out high-frequency noise in three-dimensional path-following control. However, the effects of time-varying trajectory on vehicle speed and attitude were not considered in these studies.

To overcome the uncertainty of model parameters, Aguiar, A. and Joao, P. (2007) proposed an adaptive switching control monitoring strategy, which guaranteed the system errors to be globally bounded. To avoid singularity occurrence in the line-of-sight backstepping method, Xu et al. (2014) defined multiple virtual speed error variables to help achieve three-dimensional trajectory tracking. However, the way it used to deal with singularity would degrade the control performance of the system; furthermore, the trajectory inflection point issue was not considered. K.D. Do (2015) designed a robust adaptive controller, which eliminated external disturbances and succeeded in planar trajectory tracking. In Simon. X. Yang and T. Hu (2002), Simon X. Yang et al. (2012), Chang-Zhong Pan et al. (2013), a bio-inspired model combined with backstepping was developed for mobile robots and surface ships. Because the dynamics models of these vehicles were relatively simple, their controller designs were also fairly easy to implement. Bing Sun et al. (2014a) and Bing Sun et al (2014b) successfully applied the bio-inspired model to a fully actuated manned submarine vehicle and an unmanned underwater vehicle, respectively. This method only generated smooth and filtered signals in the kinematic model without considering the dynamic model.

In this paper, a method of integrating bio-inspired models and backstepping technique is adopted to carry out three-dimensional trajectory tracking control for an underactuated AUV. The rest of this paper is organized as follows. Section 2 describes the problems of AUV modeling and coordinate transformation. Three assumptions and three bio-inspired models are proposed to support the control objects of three-dimensional trajectory tracking. Section 3 develops a three-dimensional trajectory tracking controller for underactuated AUVs with velocity regulation using Lyapunov theory and backstepping technique. Section 4 proves that the control system is uniformly ultimately bounded under constant external disturbances. Section 5 presents simulation process and discussion of the obtained results. Finally, the last section makes a summary of the three-dimensional trajectory tracking scheme and concludes its advantages.

2. Problem description

In this section, the three-dimensional kinematic and kinetic models for an underactuated AUV are established first. The conversion between earth-fixed coordinate and the body-fixed coordinate is also performed. Next, issues related to three-dimensional trajectory tracking control are addressed. The bio-inspired models used to regulate velocity error are then introduced.

2.1. Underactuated AUV modeling and coordinate transformation

This type of AUVs studied in the present work lacks sway and heave propellers. Therefore, it can be classified as a typical underactuated AUV. To better analyze the motion of AUV in the three-dimensional space, we define two coordinate systems as shown in Fig. 1E and B represent the earth-fixed coordinate system and the body-fixed coordinate system of the AUV, respectively.

The matrix-vectors of kinematic and kinetic models for AUV are:

$$\dot{\boldsymbol{\eta}} = \boldsymbol{J}(\boldsymbol{\eta})\boldsymbol{\nu} \tag{1}$$

$$\boldsymbol{M}\dot{\boldsymbol{\nu}} = \boldsymbol{\tau} + \boldsymbol{\tau}_{\omega} - \boldsymbol{C}(\boldsymbol{\nu})\boldsymbol{\nu} - \boldsymbol{D}(\boldsymbol{\nu})\boldsymbol{\nu} - \mathbf{g}(\boldsymbol{\eta}) \tag{2}$$

where $\eta = [X_E, Y_E, Z_E, \theta, \psi]^{\mathrm{T}} \in \Re^5$ denotes the AUV's position and attitude vector in earth-fixed coordinate system; $J(\eta)$ is the transformation matrix between the earth-fixed coordinate system and the body-fixed coordinate system; M is inertia matrix, including added mass; $v = [u, v, w, q, r]^{\mathrm{T}} \in \Re^5$is velocity vector in the body-fixed coordinate system; $C(v)$ is the matrix of centrifugal and Coriolis terms, including centrifugal

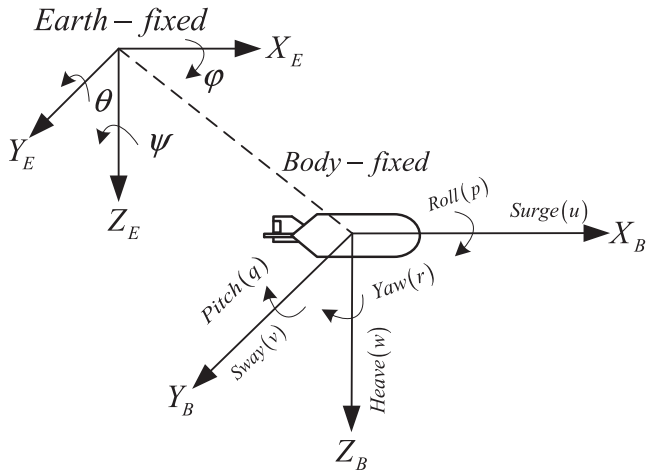

Fig. 1. AUV coordinate system.

force and Coriolis torque produced by the added mass; $D(v)$ is the damping matrix; $g(\eta)$ is the restoring force and torque vector; $\tau = [\tau_u, 0, 0, \tau_q, \tau_r]^{\mathrm{T}} \in \Re^5$ is the input vector control; $\tau_\omega = [\omega_u, \omega_v, \omega_w, \omega_q, \omega_r]^{\mathrm{T}} \in \Re^5$ is the external disturbance vector, and

$$J(\eta) = \begin{bmatrix} \cos\psi\cos\theta & \sin\psi\cos\theta & -\sin\theta & 0 & 0 \\ -\sin\psi & \cos\psi & 0 & 0 & 0 \\ \sin\theta\cos\psi & \sin\theta\sin\psi & \cos\theta & 0 & 0 \\ 0 & 0 & 0 & 1 & 0 \\ 0 & 0 & 0 & 0 & 1 \end{bmatrix} \in \Re^{5\times5}.$$

The underactuated AUV described here satisfies the following conditions: 1) the mass distribution of the vehicle is homogeneous; 2) the center of gravity coincides with the center of buoyancy; and 3) the roll motion and nonlinear hydrodynamic parameters higher than tow are neglected. The following 5-DOF model is constructed (Do, K.D and Pan, J, 2009.)

Kinematics:

$$\begin{cases} \dot{x} = u\cos\psi\cos\theta - v\sin\psi + w\cos\psi sin\theta \\ \dot{y} = u\sin\psi\cos\theta + vcos\psi + wsin\psi sin\theta \\ \dot{z} = -usin\theta + w\cos\theta \\ \dot{\theta} = q \\ \dot{\psi} = r/\cos\theta \end{cases} \tag{3}$$

Dynamics:

$$\begin{cases} m_{11}\dot{u} = m_{22}vr - m_{33}wq - d_{11}u + \tau_u + \omega_u \\ m_{22}\dot{v} = -m_{11}ur - d_{22}v + \omega_v \\ m_{33}\dot{w} = m_{11}uq - d_{33}w + \omega_w \\ m_{55}\dot{q} = (m_{33} - m_{11})uw - d_{55}q - \rho g\nabla\overline{GM_L}\sin\theta + \tau_q + \omega_q \\ m_{66}\dot{r} = (m_{11} - m_{22})uv - d_{66}r + \tau_r + \omega_r \end{cases} \tag{4}$$

where $m_{11} = m - X_{\dot{u}}$; $m_{22} = m - Y_{\dot{v}}$; $m_{33} = m - N_{\dot{r}}$; $m_{55} = I_y - M_{\dot{u}}$; $m_{66} = I_z - N_{\dot{r}}$; m denotes the mass of the vehicle; $X_{\dot{u}}$, $Y_{\dot{v}}$, $N_{\dot{r}}$ and $M_{\dot{u}}$ are added mass terms; $d_{11} = X_u + X_{u|u|}|u|$; $d_{22} = Y_v + Y_{v|v|}|v|$; $d_{33} = Z_w + Z_{w|w|}|w|$; X_u, Y_v, Z_w, M_q and $N_r$are hydrodynamic coefficients of the linear drag terms; $d_{55} = M_q + M_{q|q|}|q|$; $d_{66} = N_r + N_{r|r|}|r|$; $X_{u|u|}$, $Y_{v|v|}$, $Z_{w|w|}$, $M_{q|q|}$ and $N_{r|r|}$are the hydrodynamic coefficients of the quadratic drag terms; ρ, g, ∇, $\overline{GM_L}$ are the density of water, gravity, underwater full drainage volume, and height of initial stability, respectively; ω_u, ω_v, ω_w, ω_q, and ω_r are the components of external constant disturbance.

The desired yaw angle and pitch angle are obtained only based on the reference trajectory, where

$$\psi_d = arc\tan\frac{\dot{y}_d}{\dot{x}_d}, \theta_d = -arc\tan\frac{\dot{z}_d}{\sqrt{\dot{x}_d^2 + \dot{y}_d^2}} \tag{5}$$

The position and attitude error variables:

$$[e_x \;\; e_y \;\; e_z \;\; e_\theta \;\; e_\psi]^{\mathrm{T}} = J(\eta)[x_e \;\; y_e \;\; z_e \;\; \theta_e \;\; \psi_e]^{\mathrm{T}} \tag{6}$$

and

$$[x_e \;\; y_e \;\; z_e \;\; \theta_e \;\; \psi_e]^{\mathrm{T}} = [x - x_d \;\; y - y_d \;\; z - z_d \;\; \theta - \theta_d \;\; \psi - \psi_d]^{\mathrm{T}} \tag{7}$$

where $(x_d, \; y_d, \; z_d, \; \theta_d, \; \psi_d)$ is the position and attitude in the earth-fixed coordinate, and $(e_x, \; e_y, \; e_z, \; e_\theta, \; e_\psi)$ is the position and attitude errors in the body-fixed coordinate.

Substituting Eqs. (3), (5) into Eq. (6) yields:

$$\begin{bmatrix} \dot{e}_x \\ \dot{e}_y \\ \dot{e}_z \\ \dot{e}_\theta \\ \dot{e}_\psi \end{bmatrix} = \begin{bmatrix} u + re_y - qe_z - v_p\sin\theta_d\sin\theta - v_t\cos\theta\cos e_\psi \\ v - re_x - e_z r\tan\theta + v_t\sin e_\psi \\ w + qe_x + e_y r\tan\theta + v_p\sin\theta_d\cos\theta - v_t\sin\theta\cos e_\psi \\ q - \dot{\theta}_d \\ r\cos^{-1}\theta - \dot{\psi}_d \end{bmatrix} \tag{8}$$

where $v_p = \sqrt{\dot{x}_d^2 + \dot{y}_d^2 + \dot{z}_d^2}$, $v_t = \sqrt{\dot{x}_d^2 + \dot{y}_d^2}$.

We now make three assumptions for the underactuated AUV:

Assumption 1: The underactuated AUV's velocity and control input are bounded, i.e., $|\tau_u| \le \overline{\tau}_u$, $|\tau_q| \le \overline{\tau}_q$, $|\tau_r| \le \overline{\tau}_r$, $|u| \le \overline{u}$, $|v| \le \overline{v}$, $|w| \le \overline{w}$, $|q| \le \overline{q}$, $|r| \le \overline{r}$, where $\overline{\tau}_u$, $\overline{\tau}_q$, $\overline{\tau}_r$, $\overline{u}$, $\overline{v}$, $\overline{w}$, $\overline{q}$, $\overline{r}$ are the known upper bounds.

Assumption 2: The desired track variables u_d, q_d, r_d are bounded, and their derivatives $\dot{u}_d$, $\dot{q}_d$, $\dot{r}_d$ are also bounded, $t > 0$.

Assumption 3: The underactuated AUV's pitch angle $|\theta(t)| < \pi/2, \; \forall t \ge 0$.

2.2. Control objects

For further description, we first define the desired state of AUV as

$$X_d(t) = [x_d(t), y_d(t), z_d(t), \theta_d(t), \psi_d(t)]^T \tag{9}$$

AUV's actual state:

$$X(t) = [x(t), y(t), z(t), \theta(t), \psi(t)]^T \tag{10}$$

Considering Eqs. (1) and (2), we should design a controller such that state $X(t)$ precisely tracks the desired state $X_d(t)$:

$$\lim_{t\to\infty} X(t) = X_d(t) \tag{11}$$

2.3. Bio-inspired model

To study the occurrence and transmission process of the signals in biological neuron systems, A. L. Hodgkin and A. F. Huxley (1952) proposed the famous nerve cell membrane circuit model (H–H model). The voltage of the neurons V_m in the model satisfies the following kinetics equation:

$$C_m\frac{dV_m}{dt} = -(E_p + V_m)g_p + (E_{Na} - V_m)g_{Na} - (E_k + V_m)g_K \tag{12}$$

where C_m is the membrane capacitance; E_p, E_{Na}, E_k are Nernst potential, sodium ions, and passive ions of the membrane

current, respectively; g_p, g_{Na} and g_K are conductance of neutral channel, sodium ion, and potassium ion, respectively.

S. Grossberg (1983) further reviewed and developed the H–H model. Let coefficients of Eq. (12) be as follows:

$$C_m = 1, x_i = E_p + V_m, A = g_p, B = E_{Na} + E_p, D = E_k - E_p,$$
$$S_i^+ = g_{Na}, S_i^- = g_K.$$

Then, a bio-inspired model is obtained:

$$\frac{dx_i}{dt} = -Ax_i + (B - x_i)S_i^+(t) - (D + x_i)S_i^-(t) \tag{13}$$

where x_i represents the membrane potential (activity value) of i_{th} number neuron; parameters A, B and D are passive decay rate of the membrane potential, and upper and lower nerve excitation, respectively; Variables $S_i^+(t)$ and $S_i^-(t)$ are excitation and inhibition inputs of the i_{th} neuron.

In Eq. (13), the activity value of neuron x_i varies within the range of $[-D, B]$. For any external excitatory and inhibitory inputs, this bio-inspired model guarantees that the output values are in the bounded range. S. Grossberg (1988) has rigorously proven the stability and output boundedness of this bio-inspired model. When there is excitatory input $S_i^+(t)(S_i^+(t) \geq 0)$, neuron x_i increases and automatically obtains the control term $B - x_i$. If $x_i < B$, then $(B - x_i)S_i^+(t)$ allows neuron x_i to increase positively; if $x_i > B$, then $(B - x_i)S_i^+(t)$ becomes negative, causing neuron x_i to reach the upper limit B. On the other hand, neuron x_i reaches the lower limit $-D$ when inhibition input exists.

Given the characteristics of the bio-inspired model, such as less calculation, gain self-adjustment, and smooth and bounded output, this paper designs a three-dimensional trajectory tracking controller for underactuated AUVs with velocity regulation. Modifications are made to the existing control law of the virtual velocity error control in the backstepping approach family. Surge velocity error and angular velocity errors are considered in the bio-inspired models. By regulating the parameters of decay rate A, upper limit B, and lower limit D of the neural excitation, not only can skipping at the inflection point be efficiently suppressed, singularity problems in the existing virtual velocity control techniques are also avoided. Schematic of the designed three-dimensional underactuated AUV trajectory tracking control system with constant external disturbances is shown in Fig. 2.

3. Controller design

Based on the Lyapunov theory and backstepping technique, a three-dimensional trajectory tracking controller for underactuated AUVs with velocity regulation is designed.

Step 1: Choose a Lyapunov function candidate as follows

$$V_1(t) = \frac{1}{2}\left(e_x^2 + e_y^2 + e_z^2\right) \tag{14}$$

Combined with Eq. (8), the derivative of Eq. (14) can be obtained

$$\dot{V}_1(t) = e_x\left(u - v_p \sin\theta_d \sin\theta - v_t \cos\theta \cos e_\psi\right) + e_y(v + v_t \sin e_\psi) + e_z\left(w - v_p \sin_\theta - v_t \sin\theta(\cos e_\psi - 1)\right) \tag{15}$$

Define two virtual velocity error variables

$$\alpha = v_t \sin e_\psi, \beta = v_p \sin e_\theta \tag{16}$$

To make $\dot{V}_1(t)$ negative, the desired values u, α and β are chosen as follows

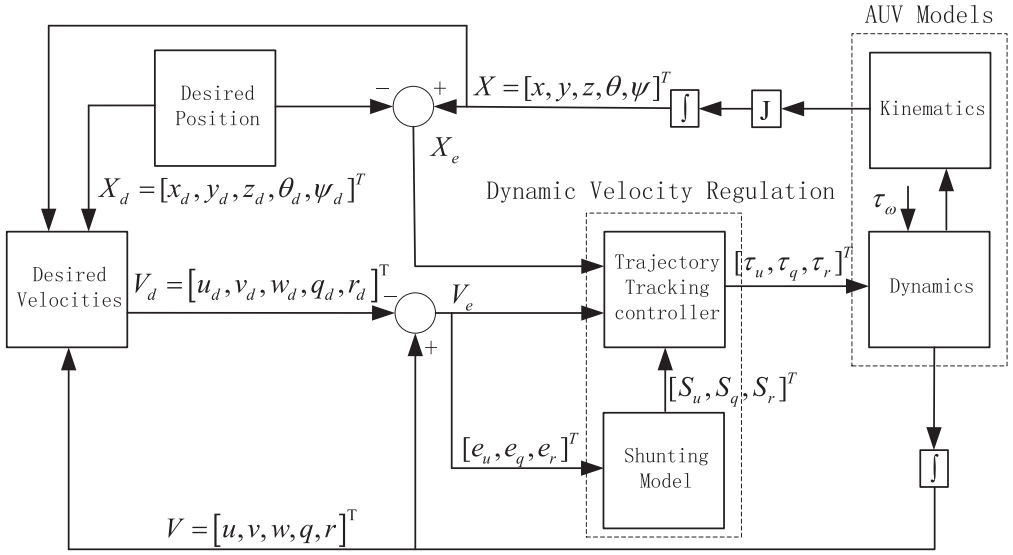

Fig. 2. Schematic of the proposed three-dimensional trajectory tracking control system.

$$\begin{cases} u_d = -k_1 e_x/e + v_p \sin\theta_d \sin\theta + v_t \cos\theta \cos e_\psi \\ \alpha_d = -k_2 e_y/e - v \\ \beta_d = k_3 e_z/e - v_t \sin\theta(\cos e_\psi - 1) + w \end{cases} \tag{17}$$

where k_1, k_2, and k_3 are all positive constants. $e = \sqrt{1 + e_x^2 + e_y^2 + e_z^2}$. It avoids that the velocities (u_d, α_d and β_d) beyond the vehicle can reach when the initial conditions e_x, e_y and e_z are too large.

Considering that u_d, α_d, β_d are not true control values, we define three error variables

$$\begin{cases} e_u = u - u_d \\ e_\alpha = \alpha - \alpha_d \\ e_\beta = \beta - \beta_d \end{cases} \tag{18}$$

Substitute Eqs. (16)–(18) into Eq. (15) yields

$$\dot{V}_1(t) = -\left(k_1 e_x^2 + k_2 e_y^2 + k_3 e_z^2\right)\Big/ e + e_u e_x + e_\alpha e_y - e_\beta e_z \tag{19}$$

Step 2: Considering Eq. (14), we choose a Lyapunov function candidate

$$V_2(t) = V_1(t) + \frac{1}{2}e_\alpha^2 + \frac{1}{2}e_\beta^2 \tag{20}$$

Its derivative becomes

$$\begin{aligned} \dot{V}_2(t) &= \dot{V}_1(t) + e_\alpha \dot{e}_\alpha + e_\beta \dot{e}_\beta \\ &= -\left(k_1 e_x^2 + k_2 e_y^2 + k_3 e_z^2\right)\Big/ e + e_u e_x + e_\alpha\left(\dot{e}_\alpha + e_y\right) \\ &\quad + e_\beta(\dot{e}_\beta - e_z) \end{aligned} \tag{21}$$

Combine Eqs. (16) and (17), and derive both sides of Eq. (18) to yield

$$\begin{cases} \dot{e}_u = \dot{u} - \dot{u}_d \\ \dot{e}_\alpha = \dot{v}_t \sin e_\psi + v_t \cos e_\psi\left(r/\cos\theta - \dot{\psi}_d\right) - \dot{\alpha}_d \\ \dot{e}_\beta = \dot{v}_p \sin e_\theta + v_p \cos e_\theta\left(q - \dot{\theta}_d\right) - \dot{\beta}_d \end{cases} \tag{22}$$

In order to make $\dot{V}_2(t)$ negative, and to avoid $\cos e_\psi$ and $\cos e_\theta$ appearing in the denominator of virtual control law using virtual velocity error and backstepping method (see Eq. (47) in appendix), we redefine the desired values r and q as follows

$$\begin{cases} r_d = \dfrac{\left(-k_4 e_\alpha - e_y + \dot{\alpha}_d - \dot{v}_t \sin e_\psi\right)\cos\theta}{v_t} + \dot{\psi}_d \cos\theta \\ q_d = \dfrac{\left(-k_5 e_\beta + e_z + \dot{\beta}_d - \dot{v}_p \sin e_\theta\right)}{v_p} + \dot{\theta}_d \end{cases} \tag{23}$$

Although XU Jian et al. (2014) eliminated the singularity problem in virtual control law r_d and q_d by removing $\cos e_\psi$ and $\cos e_\theta$ from the denominator. However, their designed controller did not consider the deterioration of the stability with it; the situation of $\cos e_\psi = \pm\pi/2$ was not given in simulations either. In order to overcome this shortcoming, this paper uses the characteristics of the bio-inspired model to regulate dynamic velocity error. Thus, issues of skipping at inflection points can be better inhibited. By using the controller designed in this paper, singularity can be avoided, right angle inflection point skip issue is resolved, and performance of the system control is improved. Simulation results are given in Appendix for the case of $\cos e_\psi$ and $\cos e_\theta$ appearing in the virtual control law denominator r_d and q_d using the controller designed in this paper. The process is also further explained in Appendix, where k_4, k_5 are positive constants; considering q_d and r_d are not true controllable variables, error variables are defined

$$\begin{cases} e_r = r - r_d \\ e_q = q - q_d \end{cases} \tag{24}$$

Substituting Eqs. (22)–(24) into Eq. (21), the equation can be rewritten as

$$\begin{aligned} \dot{V}_2(t) = &-\left(k_1 e_x^2 + k_2 e_y^2 + k_3 e_z^2\right)\Big/ e - k_4 e_\alpha^2 - k_5 e_\beta^2 + e_u e_x \\ &+ \frac{e_\alpha v_t}{\cos\theta}(e_r \cos e_\psi + \delta_1) + e_\beta v_p\left(e_q \cos e_\theta + \delta_2\right) \end{aligned} \tag{25}$$

where
$\delta_1 = (r_d - \dot{\psi}_d \cos\theta)(\cos e_\psi - 1), \delta_2 = (q_d - \dot{\theta}_d)(\cos e_\theta - 1)$.

In order to achieve a better control effect, in the next step we will substitute surge velocity error and angular velocity error into the bio-inspired models to realize dynamic regulation.

Step 3: Consider the following Lyapunov function candidate

$$V_3(t) = V_2(t) + \frac{1}{2}\left(e_u^2 + e_q^2 + e_r^2\right) \tag{26}$$

Calculating the derivative of Eq. (26) along Eqs. (23) and (24) yields

$$\begin{aligned} \dot{V}_3(t) &= \dot{V}_2(t) + e_u \dot{e}_u + e_q \dot{e}_q + e_r \dot{e}_r \\ &= -\left(k_1 e_x^2 + k_2 e_y^2 + k_3 e_z^2\right)\Big/ e - k_4 e_\alpha^2 - k_5 e_\beta^2 + e_u(e_x + \dot{e}_u) \\ &\quad + e_r\left(e_\alpha v_t \cos e_\psi \cos^{-1}\theta + \dot{e}_r\right) + e_q\left(e_\beta v_p \cos e_\theta + \dot{e}_q\right) + \delta \end{aligned} \tag{27}$$

where $\delta = e_\alpha v_t \delta_1 \cos^{-1}\theta + e_\beta v_p \delta_2$.

Substitute surge velocity error e_u, pitch angular velocity error e_q, and yaw angular velocity e_r into the bio-inspired models, respectively, we get

$$\begin{aligned} \dot{S}_i &= -A_j S_i + \left(B_j - S_i\right) f(e_i) - \left(D_j + S_i\right) g(e_i) \\ &= -\left[A_j + f(e_i) + g(e_i)\right] S_i + \left[B_j f(e_i) - D_j g(e_i)\right] \end{aligned} \tag{28}$$

where $(i = u, q, r; j = 1, 2, 3)$; S_u, S_q and S_r are outputs of the dynamic model, defined as surge, pitch angular and yaw angular velocity errors, respectively; parameters A_j is a nonnegative constant representing the passive decay rates of outputs for dynamic velocity errors; constants B_j and D_j are the upper and lower limits of outputs for dynamic velocity errors; $f(e_i) = \max\{e_i, 0\}$, $g(e_i) = \max\{-e_i, 0\}$.

We choose dynamic velocity regulation control laws τ_u, τ_q and τ_r as

$$\begin{cases} \tau_u = m_{11}(\dot{u}_d - f_u - e_x - S_u) - \widehat{\omega}_u \\ \tau_q = m_{55}\left(\dot{q}_d - f_q - \dfrac{e_\alpha v_t \cos e_\psi}{\cos\theta} - S_q\right) - \widehat{\omega}_q \\ \tau_r = m_{66}\left(\dot{r}_d - f_r - e_\beta v_p \cos e_\theta - S_r\right) - \widehat{\omega}_r \end{cases} \tag{29}$$

where

$$\begin{cases} f_u = (m_{22}vr - m_{33}wq - d_{11}u)m_{11}^{-1} \\ f_q = \left[(m_{33} - m_{11})uw - d_{55}q - \rho g\nabla\overline{GM_L}\sin\theta\right]m_{55}^{-1} \\ f_r = [(m_{11} - m_{22})uv - d_{66}r]m_{66}^{-1} \end{cases} \tag{30}$$

Substituting Eqs. (28)−(30) into Eq. (27), it can be re-written as

$$\begin{aligned} \dot{V}_3(t) = &-\left(k_1e_x^2 + k_2e_y^2 + k_3e_z^2\right)\Big/e - k_4e_\alpha^2 - k_5e_\beta^2 - S_ue_u - S_qe_q \\ &- S_re_r + e_u\tilde{\omega}_u + e_q\tilde{\omega}_q + e_r\tilde{\omega}_r + \delta \end{aligned} \tag{31}$$

where $\tilde{\omega}_i = \omega_i - \widehat{\omega}_i$, $(i = u, q, r)$, $\widehat{\omega}_u$, $\widehat{\omega}_q$, and $\widehat{\omega}_r$ are the estimated values of disturbances.

Step 4: Consider a Lyapunov function

$$V_4(t) = V_3(t) + \frac{1}{2}\left(\frac{1}{B_1}S_u^2 + \frac{1}{B_2}S_q^2 + \frac{1}{B_3}S_r^2\right) \tag{32}$$

Evaluating its time derivative yields

$$\begin{aligned} \dot{V}_4(t) &= \dot{V}_3(t) + \frac{1}{B_1}S_u\dot{S}_u + \frac{1}{B_2}S_q\dot{S}_q + \frac{1}{B_3}S_r\dot{S}_r \\ &= -\left(k_1e_x^2 + k_2e_y^2 + k_3e_z^2\right)\Big/e - k_4e_\alpha^2 - k_5e_\beta^2 + e_u\tilde{\omega}_u + e_q\tilde{\omega}_q \\ &\quad + e_r\tilde{\omega}_r + \delta + \frac{1}{B_1}S_u\left(\dot{S}_u - B_1e_u\right) + \frac{1}{B_2}S_q\left(\dot{S}_q - B_2e_q\right) \\ &\quad + \frac{1}{B_3}S_r\left(\dot{S}_r - B_3e_r\right) \end{aligned} \tag{33}$$

Combined with Eq. (28), the following equation can be obtained

$$\begin{aligned} \dot{V}_4(t) = &-\left(k_1e_x^2 + k_2e_y^2 + k_3e_z^2\right)\Big/e - k_4e_\alpha^2 - k_5e_\beta^2 - A_uS_u^2 \\ &- A_qS_q^2 - A_rS_r^2 + B_uS_u + B_qS_q + B_rS_r + e_u\tilde{\omega}_u + e_q\tilde{\omega}_q \\ &+ e_r\tilde{\omega}_r + \delta \end{aligned} \tag{34}$$

where
$A_i = B_j^{-1}[A_j + f(e_i) + g(e_i)], B_i = B_j^{-1}[B_jf(e_i) - D_jg(e_i) - B_je_i](i = u, q, r; j = 1, 2, 3)$.

Finally, we obtain the error equations of the trajectory tracking system as following

$$\begin{cases} \dot{x}_e = -k_1e_x/e + e_u + re_y - qe_z \\ \dot{y}_e = -k_2e_y/e + e_\alpha - re_x - e_zr\tan\theta \\ \dot{z}_e = -k_3e_z/e - e_\beta + qe_x + e_yr\tan\theta \\ \dot{e}_\alpha = -k_4e_\alpha - e_y + \dfrac{v_t(e_r\cos e_\psi + \delta_1)}{\cos\theta} \\ \dot{e}_\beta = -k_5e_\beta - e_z + v_p\left(e_q\cos e_\theta + \delta_2\right) \\ \dot{e}_u = -S_u - x_e + \tilde{\omega}_u \\ \dot{e}_q = -S_q - \dfrac{e_\alpha v_t\cos e_\psi}{\cos\theta} + \tilde{\omega}_q \\ \dot{e}_r = -S_r - e_\beta v_p\cos e_\theta + \tilde{\omega}_r \end{cases} \tag{35}$$

4. Proof of stability

Theorem 1: On the premise of Assumptions 1 and 2, we consider the models represented by Eqs. (3) and (4) with external disturbances. If the trajectory tracking controller is chosen as Eq. (29), then the closed loop system (Eq. (35)) is uniformly ultimately bounded.

Proof: Let $B_j = D_j(j = 1, 2, 3)$,

If $e_i > 0$, then $f(e_i) = e_i$, $g(e_i) = 0$, and

$$f(e_i) - g(e_i) - e_i = 0 \tag{36}$$

If $e_i < 0$, then $f(e_i) = 0$, $g(e_i) = e_i$, and

$$f(e_i) - g(e_i) - e_i = 0 \tag{37}$$

where $(i = u, q, r)$.

Therefore, $B_u = 0$, $B_q = 0$, $B_r = 0$.

Combined with Eqs. (36) and (37), Eq. (34) can be calculated as

$$\begin{aligned} \dot{V}_4(t) = &-\left(k_1e_x^2 + k_2e_y^2 + k_3e_z^2\right)\Big/e - k_4e_\alpha^2 - k_5e_\beta^2 - A_uS_u^2 \\ &- A_qS_q^2 - A_rS_r^2 + e_u\tilde{\omega}_u + e_q\tilde{\omega}_q + e_r\tilde{\omega}_r + \delta \end{aligned} \tag{38}$$

From the definitions of $f(\cdot)$ and $g(\cdot)$, it can be known that $f(\cdot) \geq 0$ and $g(\cdot) \geq 0$. As the parameters A_j, B_j, $D_j(j = 1, 2, 3)$ are nonnegative constants, we have $A_i \geq 0(i = u, q, r)$.where $A_u = B_1^{-1}[A_1 + f(e_u) + g(e_u)]$, $A_q = B_2^{-1}[A_2 + f(e_q) + g(e_q)]$,$A_r = B_3^{-1}[A_3 + f(e_r) + g(e_r)]$.

Furthermore, we design another Lyapunov function

$$V_5 = V_4 + \frac{1}{2}\left(c_1\tilde{\omega}_u^2 + c_2\tilde{\omega}_q^2 + c_3\tilde{\omega}_r^2\right) \tag{39}$$

where c_1, c_2, c_3 are positive constants.

Then, its derivative becomes

$$\begin{aligned}\dot{V}_5(t) &= \dot{V}_4(t) + c_1\tilde{\omega}_u\dot{\tilde{\omega}}_u + c_2\tilde{\omega}_q\dot{\tilde{\omega}}_q + c_3\tilde{\omega}_r\dot{\tilde{\omega}}_r \\ &= -\left(k_1e_x^2 + k_2e_y^2 + k_3e_z^2\right)\Big/e - k_4e_\alpha^2 - k_5e_\beta^2 - A_uS_u^2 \\ &\quad - A_qS_q^2 - A_rS_r^2 + \tilde{\omega}_u\left(e_u + c_1\dot{\tilde{\omega}}_u\right) + \tilde{\omega}_q\left(e_q + c_2\dot{\tilde{\omega}}_q\right) \\ &\quad + \tilde{\omega}_r\left(e_r + c_3\dot{\tilde{\omega}}_r\right) + \delta\end{aligned} \tag{40}$$

According to Eq. (40), three adaptive laws for the external constant disturbances are designed

$$\begin{cases}\dot{\tilde{\omega}}_u = -\tilde{\omega}_u - e_u/c_1 \\ \dot{\tilde{\omega}}_q = -\tilde{\omega}_q - e_q/c_2 \\ \dot{\tilde{\omega}}_r = -\tilde{\omega}_r - e_r/c_3\end{cases} \tag{41}$$

Substitute Eq. (41) into Eq. (40), we get

$$\begin{aligned}\dot{V}_5 &= -\left(k_1e_x^2 + k_2e_y^2 + k_3e_z^2\right)\Big/e - k_4e_\alpha^2 - k_5e_\beta^2 - A_uS_u^2 - A_qS_q^2 \\ &\quad - A_rS_r^2 - c_1\tilde{\omega}_u^2 - c_2\tilde{\omega}_q^2 - c_3\tilde{\omega}_r^2 + \delta\end{aligned} \tag{42}$$

where the parameters k_1, k_2, k_3, k_4, k_5 and c_1, c_2, c_3 are all positive constants, and $A_i \geq 0 (i = u, q, r)$.

Therefore, under Assumptions 1 and 2, the maximum value of $\delta = e_\alpha v_t\delta_1 \cos^{-1}\theta + e_\beta v_p\delta_2$ exists, which means δ is bounded.

Define-
$z = (e_x/\sqrt{e}, e_y/\sqrt{e}, e_z/\sqrt{e}, e_\alpha, e_\beta, S_u, S_q, S_r, \tilde{\omega}_u, \tilde{\omega}_q, \tilde{\omega}_r)^{\mathrm{T}}$,
together with Eq. (42), we obtain

$$2V_5 = \|z\|^2 \tag{43}$$

Using Eq. (39), we have

$$\dot{V}_5(t) \leq -2\gamma V_5 + \delta \tag{44}$$

where $\gamma = \min\{\mathrm{k_1}, \mathrm{k_2}, \mathrm{k_3}, \mathrm{k_4}, \mathrm{A_u}, \mathrm{A_q}, \mathrm{A_r}, \mathrm{c_1}, \mathrm{c_2}, \mathrm{c_3}\}$.

By knowing that δ is bounded, we can arrive at the following equation according to the comparison principle defined by Aguiar, A. and Joao, P (2007).

$$V_5(t) \leq V_5(0)e^{-2\gamma t} + \frac{\delta}{2\gamma} \tag{45}$$

Therefore

$$\|z(t)\| \leq \|z(0)\|e^{-\gamma t} + \sqrt{\frac{\delta}{\gamma}}, \forall t > 0 \tag{46}$$

It is shown that the Lyapunov function V_5 will remain in the range $(0, \delta/2\gamma)$. Moreover, by increasing gains $k_1, k_2, k_3, k_4, A_u, A_q, A_r, c_1, c_2, c_3$, a larger γ can be obtained, which means that all the error signals are uniformly ultimately bounded.

5. Simulation and discussion

In order to verify the effectiveness and advantages of the proposed control method, a three-dimensional time-varying trajectory is designed, which includes a spiral dive and a planar trajectory. Additionally, the singularity problem is considered when yaw angle error is $\pm 90^\circ$ during trajectory tracking. The spiral dive part of the desired trajectory is described as:

$$\begin{cases}x_d = 100\sin(0.01t) \\ y_d = 100\cos(0.01t) \\ z_d = 0.1t\end{cases}$$

The starting point is $(x_0, y_0, z_0) = (10, 90, 10)$, so the initial position error is $(x_e, y_e, z_e) = (10, -10, 10)$; the initial attitudes are $(\theta_0, \psi_0) = (0, 0)$ and velocities are $(u_0, v_0, w_0, q_0, r_0) = (0, 0, 0, 0, 0)$. The trajectory equations and switching points on the desired trajectory are selected as below.

a: $(x_\mathrm{a}, y_\mathrm{a}, z_\mathrm{a}) = (-54.4, -84.0, 100)$, **b**: $(x_\mathrm{b}, y_\mathrm{b}, z_\mathrm{b}) = (-104.4, -84.0, 100)$

c: $(x_\mathrm{c}, y_\mathrm{c}, z_\mathrm{c}) = (-104.4, 66.0, 100)$, **d**: $(x_\mathrm{d}, y_\mathrm{d}, z_\mathrm{d}) = (-154.4, 66, 100)$

e: $(x_\mathrm{e}, y_\mathrm{e}, z_\mathrm{e}) = (-154.4, -84.0, 100)$, **f**: $(x_\mathrm{f}, y_\mathrm{f}, z_\mathrm{f}) = (-204.4, -84.0, 100)$.

$$0 \leq t < 1000 \begin{cases}x_d = 100Sin0.01t \\ y_d = 100Cos0.01t \\ z_d = 0.1t\end{cases}, \quad 1000 \leq t < 1050 \begin{cases}x_d = -54.4 + 1000 - t \\ y_d = -84 \\ z_d = 100\end{cases}, \quad 1050 \leq t < 1200 \begin{cases}x_d = -104.4 \\ y_d = 66 \\ z_d = 100\end{cases},$$

$$1200 \leq t < 1250 \begin{cases}x_d = -104.4 + 1200 - t \\ y_d = 66 \\ z_d = 100\end{cases}, \quad 1250 \leq t < 1400 \begin{cases}x_d = -154.1 \\ y_d = 66 + 1250 - t \\ z_d = 100\end{cases},$$

$$1400 \leq t < 1450 \begin{cases}x_d = -154.1 + 1400 - t \\ y_d = -84 \\ z_d = 100\end{cases}, \quad 1450 \leq t < 1600 \begin{cases}x_d = -204 \\ y_d = -84 - 1450 + t \\ z_d = 100\end{cases}$$

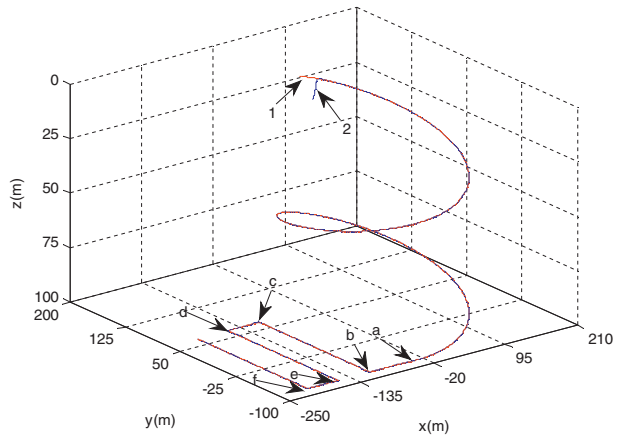

1-Desired trajectory 2-Actual trajectory

Fig. 3. Response of three-dimensional tracking.

The control gains are chosen as:$k_1 = 2$, $k_2 = 0.5$, $k_3 = 1$,$k_4 = 0.5$, $c_1 = 0.5$, $c_2 = 0.1$, $c_3 = 0.1$. The parameters of the three bio-inspired models are selected as

$$\begin{cases} A_1 = 12; B_1 = D_1 = 10 \\ A_2 = 14.5; B_2 = D_2 = 9 \\ A_3 = 14; B_3 = D_3 = 9.5 \end{cases}$$

The parameters of the underactuated AUV are listed as in K. Y. Pettersen and O. Egeland (1999):$m = 185\ kg$, $I_z = 50\ kgm^2$, $X_{\dot{u}} = -30\ kg$, $Y_{\dot{v}} = -80\ kg$, $N_{\dot{r}} = -30\ kg$, $X_u = 70\ kg/s$, $X_{u|u|} = 100\ kg/s$, $Y_v = 100\ kg/m$, $Y_{v|v|} = 200\ kg/m$, $Z_w = 100\ kg/s$, $Z_{w|w|} = 200\ kg/s$, $N_r = 50\ kgm^2/s$, $N_{r|r|} = 100\ kgm^2$, $M_q = 50\ kgm^2/s$, $M_{q|q|} = 100\ kgm^2$. The external constant disturbances are:$\omega_u = 0.5\ N$, $\omega_v = 0N$, $\omega_w = 0N$, $\omega_q = 0.1\ Nm$, $\omega_r = 0.1\ Nm$. The simulation results are shown from Fig. 3 to Fig. 15.

As shown in Fig. 3, the underactuated AUV has achieved a three-dimensional trajectory tracking mission. To further illustrate the tracking results, Figs. 4 and 7 show plane projections of XY and XZ for tracking three-dimensional trajectory, respectively. Figs. 5 and 6 are the 10-times magnification of points **c** and **d** in XY plane projection for tracking three-dimensional trajectory, respectively. As seen from the figures, when the switching point becomes a right angle, the tracking error remains within 2 m relative to the desired trajectory. This suggests that the designed controller is effective in suppressing the skip problem at inflection points.

From Figs. 8 and 9, it is shown that the tracking errors are low enough and ultimately approach zero. In Fig. 8, $E = \sqrt{e_x^2 + e_y^2 + e_z^2}$ is calculated to observe the overall error value between the desired and actual trajectories. The 5 yaw angle errors $e_\psi = \pm\pi/2$ can be seen clearly. It is displayed that the position errors approach zero quickly in Fig. 9. This also demonstrates the effectiveness and robustness of the proposed control method.

The line velocity responses of the vehicle are shown in Fig. 10, which illustrates that even with a sudden change in the curve, the velocity variations are moderate. It is demonstrated that the proposed method has successfully solved the problem of sudden velocity change. Fig. 11 indicates angular velocity responses of the vehicle. Although there is a greater alteration during sudden angular change, small tracking errors are still achieved. Fig. 12 displays the responses of actual control inputs.

Figs. 13–15 show the errors of longitudinal velocity, pitch angle velocity, yaw angle velocity, as well as their outputs of bio-inspired models, respectively. It is indicated that the dynamic velocity regulation is effective in adjusting the velocity errors. Fig. 13 shows the overshoot for surge velocity error at inflection point has been reduced by about 25%. The overshoot for pitch angle velocity error from spiral dive to planar

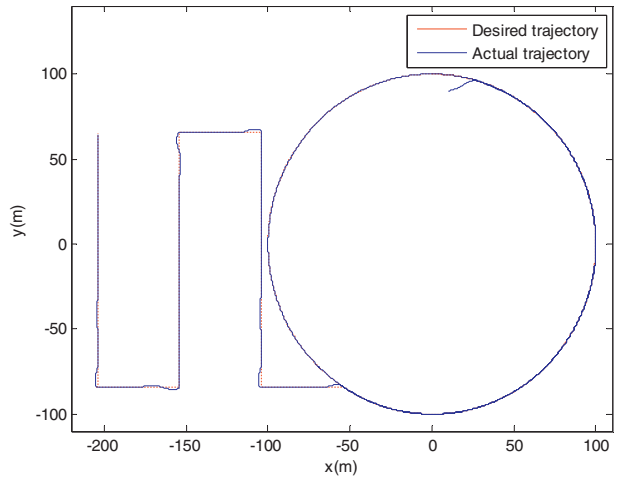

Fig. 4. Three-dimensional tracking in XY plane projection.

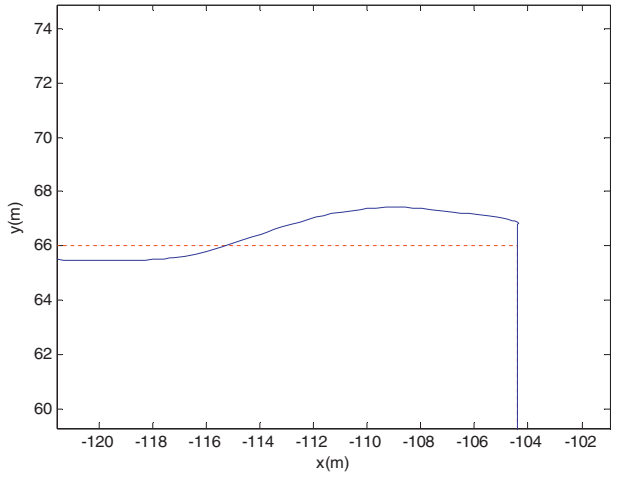

Fig. 5. Magnification of point c in XY plane projection.

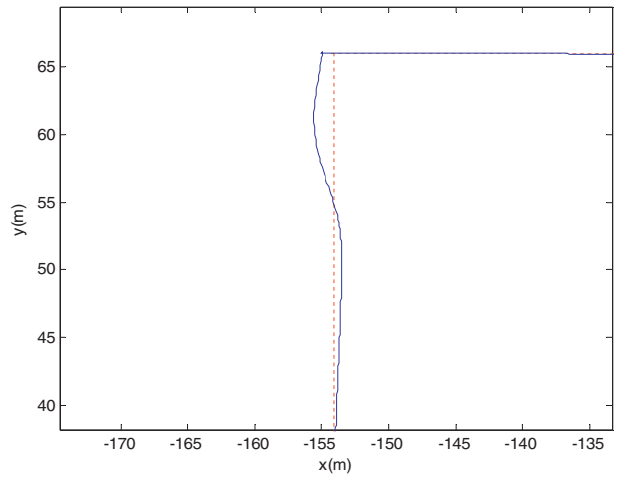

Fig. 6. Magnification of point d in XY plane projection.

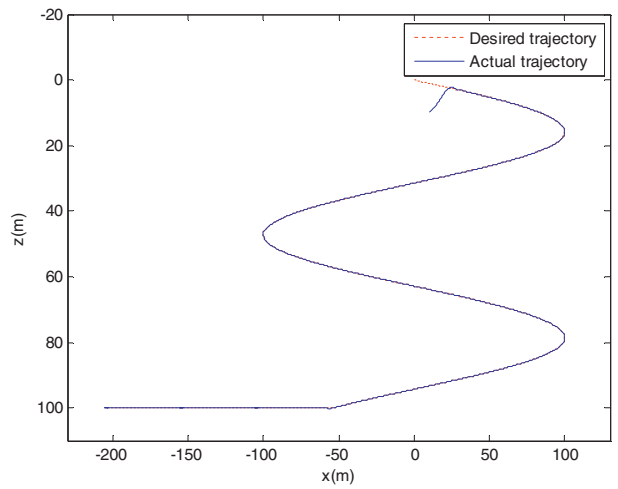

Fig. 7. Three-dimensional tracking in XZ plane projection.

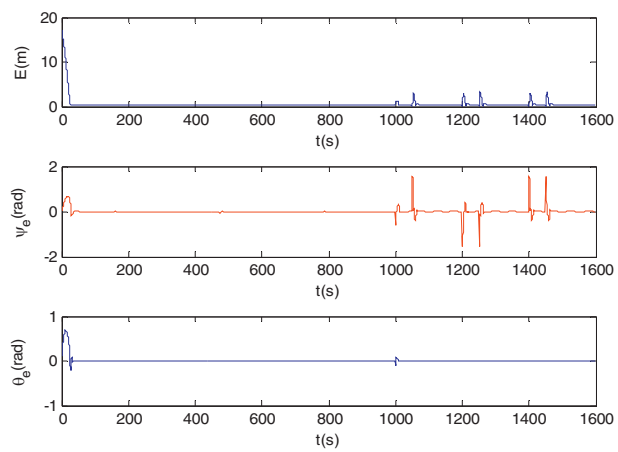

Fig. 8. The overall position error and attitude errors.

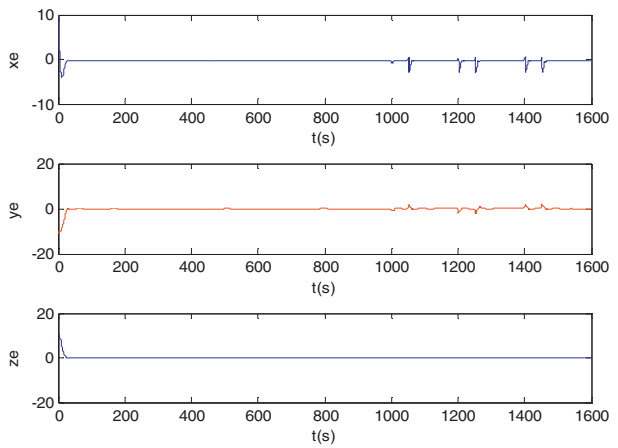

Fig. 9. Position errors of three-dimensional tracking.

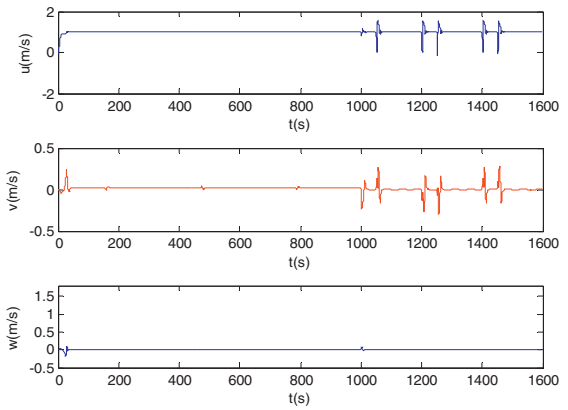

Fig. 10. Responses of line velocity.

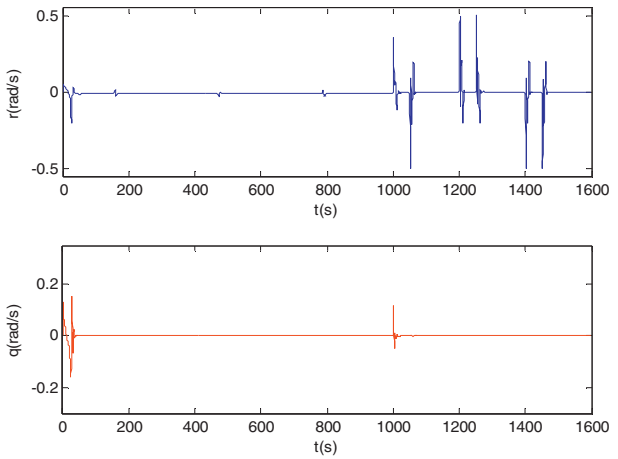

Fig. 11. Responses of angular velocity.

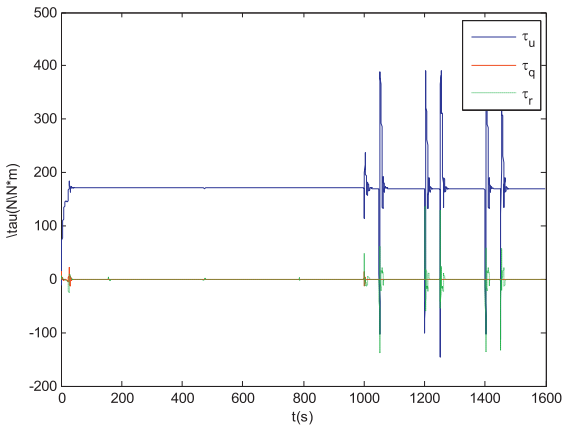

Fig. 12. Actual control inputs for the vehicle.

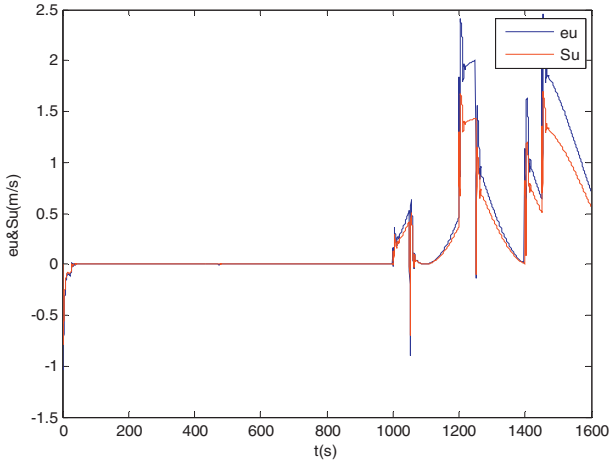

Fig. 13. Surge velocity error and its regulated output.

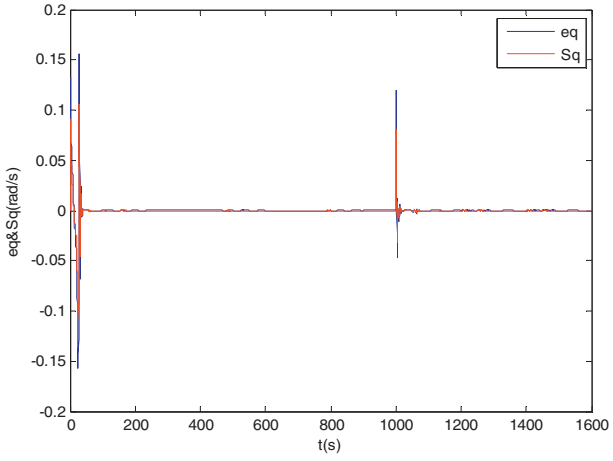

Fig. 14. Pitch angle velocity error and its regulated output.

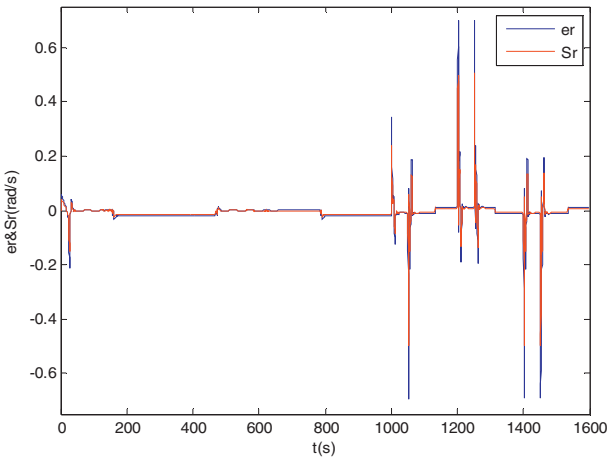

Fig. 15. Yaw angle velocity error and its regulated output.

trajectory has been reduced by about 28%, as shown in Fig. 14. It can be observed from Fig. 15 that the maximum overshoot of yaw angle velocity error at each inflection point is reduced by about 26%. The outputs of each velocity error become smaller after regulation.

From Figs. 3–15, it is clear that the proposed dynamic velocity control for trajectory tracking of underactuated AUV can be implemented under constant external disturbances, achieving precise tracking of three-dimensional trajectories.

6. Conclusion

In this work, based on the study of three-dimensional trajectory tracking of an underactuated AUV, a combination of bio-inspired model with virtual velocity variables in backstepping is innovatively adopted. At the dynamic level, a trajectory tracking controller is designed to dynamically regulate velocity variables. Not only can the controller overcome the skipping problem at inflection points, it can also avoid the singularity issue when yaw angle error is $\pm 90^{\circ}$. It reduces the error overshoots of surge velocity, pitch angle velocity, and yaw angle velocity. The states of the underactuated AUV and associated time constraints are satisfied in three-dimensional trajectory tracking. By using Lyapunov stability theory, the system is proved to be stable and robust under external constant disturbances. Finally, the simulation results show a satisfactory three-dimensional tracking accuracy with high robustness.

Acknowledgement

This work is supported by the Harbin Science and Technology Bureau under Grant 2016RAQXJ080, the National Natural Science Foundation of China under Grant 51609048, the Heilongjiang Province Science Foundation for Youths under Grant QC2017051, the Fundamental Research Funds for the Central Universities under Grant HEUCFM170402.

Appendix.

In this part, we introduce a controller using a bio-inspired model (Xu et al., 2014). The backstepping control laws of virtual velocity error variables are

$$\begin{cases} r'_d = \dfrac{\left(-l_4 e_\alpha - e_y + \dot{\alpha}_d - \dot{v}_t \sin e_\psi\right)\cos\theta}{v_t \cos e_\psi} + \dot{\psi}_d \cos\theta \\ q'_d = \dfrac{\left(-l_5 e_\beta + e_z + \dot{\beta}_d - \dot{v}_p \sin e_\theta\right)}{v_p \cos e_\theta} + \dot{\theta}_d \end{cases} \tag{47}$$

Similarly, error variables are given

$$\begin{cases} e'_r = r - r'_d \\ e'_q = q - q'_d \end{cases} \tag{48}$$

For the above mentioned Lyapunov function $V_2(t)$, substituting Eqs. (47) and (48) into Eq. (21), we can obtain

$$\begin{aligned} \dot{V}'_2(t) = &-\left(l_1 e_x^2 + l_2 e_y^2 + l_3 e_z^2\right)\Big/ e - l_4 e_\alpha^2 - l_5 e_\beta^2 + e'_u e_x \\ &+ e_\alpha v_t e'_r \cos^{-1}\theta \cos e_\psi + e_\beta v_p e'_q \cos e_\theta \end{aligned} \tag{49}$$

Define a Lyapunov function

$$V'_3(t) = V'_2(t) + \frac{1}{2}\left(e'^2_u + e'^2_q + e'^2_r\right) \tag{50}$$

Then, the time derivative of $V'_3(t)$ gives

$$\begin{aligned} \dot{V}'_3(t) = &-\left(l_1 e_x^2 + l_2 e_y^2 + l_3 e_z^2\right)\Big/ e - l_4 e_\alpha^2 - l_5 e_\beta^2 + e'_u\left(x_e + \dot{e}'_u\right) \\ &+ e'_r\left(e_\alpha v_t \cos e_\psi \cos^{-1}\theta + \dot{e}'_r\right) + e'_q\left(e_\beta v_p \cos e_\theta + \dot{e}'_q\right) \end{aligned} \tag{51}$$

Velocity error e'_u and angular velocity errors e'_q, e'_r are regulated by the bio-inspired model, as shown in Eq. (28).

Using the same method mentioned in the paper, we can get control inputs τ'_u, τ'_q and τ'_r as follows

$$\begin{cases} \tau'_u = m_{11}\left(\dot{u}'_d - x_e - S_u\right) - \widehat{\omega}_u - m_{22} vr + m_{33} wq + d_{11} u \\ \tau'_q = m_{55}\left(\dot{q}'_d - e_\alpha v_t \cos e_\psi \cos^{-1}\theta - S_q\right) - \widehat{\omega}_q - (m_{33} - m_{11})uw + d_{55} q + \rho g \nabla \overline{GM_L} \sin\theta \\ \tau'_r = m_{66}\left(\dot{r}'_d - e_\beta v_p \cos e_\theta - S_r\right) - \widehat{\omega}_r - (m_{11} - m_{22})uv + d_{66} r \end{cases} \tag{52}$$

The other Lyapunov functions for the stability analysis of this control system are chosen the same as mentioned in the paper. Tracking errors of this closed loop system can be proven to be asymptotically stable. In order to illustrate the advantage of the control laws expressed in Eq. (23), simulations are carried out using controller Eq. (52).

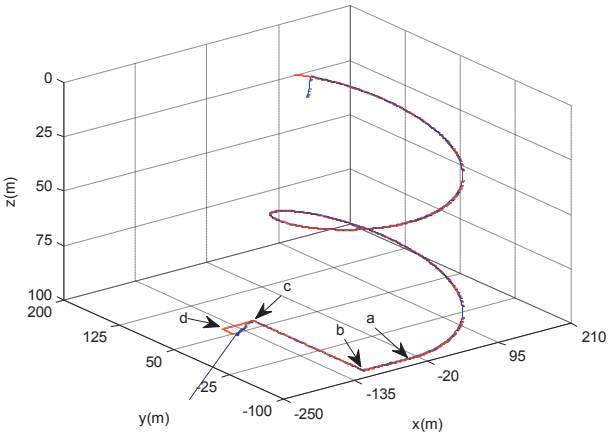

Fig. 16. Response of three-dimensional tracking.

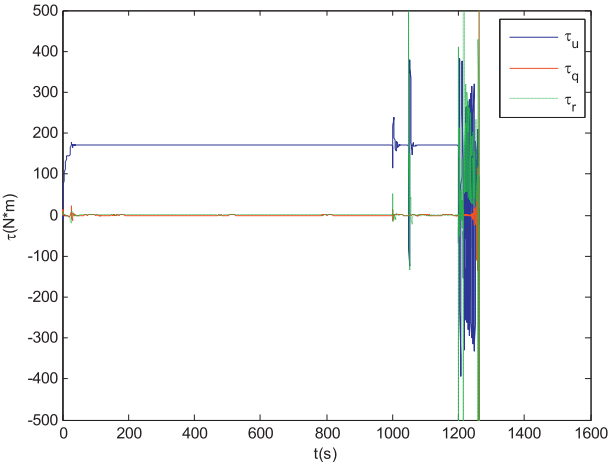

Fig. 17. Actual control inputs for the vehicle.

It is shown in Fig. 16 that the tracking overshoot is relatively small when the yaw angle error is designed to be 89° at inflection point **b**. Intentionally, when the yaw angle errors are set to be 90° at inflection points **c** and **d**, we can see that the actual trajectory would diverge from the desired one immediately, which is caused by singularity. Fig. 17 presents that

the rudder and propeller control values will chatter corresponding to the trajectory tracking at 1200s when the desired trajectory can no longer be tracked by the vehicle.

References

Aguiar, A., Joao, P., 2007. Trajectory-tracking and path-following of underactuated autonomous vehicles with parametric modeling uncertainty. IEEE Trans. Autom. Control 52 (8), 1362−1379.

Bi, F.Y., Wei, Y.J., Zhang, J.Z., Cao, W., 2010. Position-tracking control of underactuated autonomous underwater vehicles in the presence of unknown ocean currents. IET Control Theory Appl. 4 (11), 2369−2380.

Do, K.D., 2015. Control of fully actuated ocean vehicles under stochastic environmental loads in three dimensional space. Ocean Eng. 99, 34−43.

Do, K.D., 2015. Robust adaptive tracking control of underactuated ODINs under stochastic sea loads. Robotics Aut. Syst. 2015 (72), 152−163.

Do, K.D., Pan, J., 2009. Control of Ships and Underwater Vehicles: Design for Underactuated and Nonlinear Marine Systems. Springer, London, UK.

Elmokadem, Taha, Zribi, Mohamed, Youcef-Toumi, Kamal, 2016. Trajectory tracking sliding mode control of underactuated AUVs. Nonlinear Dyn. 84 (2), 1079−1091.

Fossen, Thor I., 2011. Handbook of Marine Craft Hydrodynamics and Motion Control. A John Wiley& Sons, Ltd., Publication.

Fossen, T.I., Pettersen, K.Y., Galeazzi, R., 2015. Line-of-sight path following for Dubins paths with adaptive sideslip compensation of drift forces. IEEE Trans. Control Syst. Technol. 23 (2), 820−827.

Grossberg, S., 1983. Absolute stability of global pattern formation and parallel memory storage by compective neural networks. IEEE Trans. Syst Man Cybern. 13 (5), 815−826.

Grossberg, S., 1988. Nonlinear neural networks: principles, mechanisms, and architecture. Neural Netw. 1 (1), 17−61.

He-ming, Jia, Li-jun, Zhang, Xiang-qin, Cheng, Xin-qian, Bian, Zheping, Yan, Zhou, Jiajia, 2012. Three-dimensional path following control for an underactuated AUV based on nonlinear iterative sliding mode. Acta Autom. Sin. 38 (2), 308−314.

He-ming, Jia, Xiang-qin, Cheng, Li-jun, Zhang, Xin-qian, Bian, Zheping, Yan, 2012. Three-dimensional path tracking control for underactuated AUV based on adaptive backstepping. Control Decis. 27 (5), 652−664.

Hodgkin, A.L., Huxley, A.F., 1952. A quantitative description of membrane current and its application to conduction and excitation in nerve. J. Physiol. 117 (4), 500−544.

Hong-Jian, Wang, Zi-Yin, Chen, He-Ming, Jia, Li, Juan, 2015. Three-dimensional path-following control of underactuated autonomous underwater vehicle with command filtered backstepping. Acta Autom. Sin. 41 (3), 631−645.

Kim, Do Wan, 2015. Tracking of REMUS autonomous underwater vehicles with actuator saturations. Automatica 58, 15−21.

Pan, Chang-Zhong, Lai, Xu-Zhi, Yang, Simon X., Wu, Min, 2013. An efficient neural network approach to tracking control of an autonomous surface vehicle with unknown dynamics. Expert Syst. Appl. 40, 1629−1635.

Pettersen, K.Y., Egeland, O., 1999. Time-varying exponential stabilization of the position and attitude of an underactuated autonomous underwater vehicle. IEEE Trans. Autom. Control 44 (1), 112−115.

Simon, X., Yang, T. Hu, 2002. An efficient neural network approach to real-time control of a mobile robot with unknown dynamics. Differ. Equ. Dyn. Syst. 1 (10), 151−168.

Sun, Bing, Zhu, Daqi, Yang, Simon X., 2014. A bioinspired filtered backstepping tracking control of 7000-m manned submarine vehicle. IEEE Trans. Ind. Electron. 61 (7), 3682−3693.

Sun, Bing, Zhu, Daqi, Yang, Simon X., 2014. A bio-inspired cascaded approach for three-dimensional tracking control of unmanned underwater vehicles. Int. J. Robot. Automat. 29 (4), 349−358.

Sun, Yu-shan, Ran, Xiang-rui, Li, Yue-ming, Zhang, Guo-cheng, Zhang, Yinghao, 2016. Thruster fault diagnosis method based on Gaussian particle filter for autonomous underwater vehicles. Int. J. Nav. Archit. Ocean Eng. 8, 243−251.

Xu, Jian, Wang, Man, Qiao, Lei, 2014. Backstepping-based controller for three-dimensional trajectory tracking of underactuated underwater vehicles. Control Theory Appl. 31 (11), 1589−1596.

Yan, Zheping, Yu, Haomiao, Zhang, Wei, Li, Benyin, Zhou, Jiajia, 2015. Globally finite-time stable tracking control of underactuated AUVs. Ocean Eng. 107, 132−146.

Yang, Simon X., Zhu, Anmin, Yuan, Guangfeng, Meng, Max Q.-H., 2012. A bioinspired neurodynamics-based approach to tracking control of mobile robots. IEEE Trans. Ind. Electron. 59 (8), 3211−3220.

Zhou, Jiajia, Tang, Zhaodong, Zhang, Honghan, Jiao, Jianfang, 2013. Spatial path following for AUVs using adaptive neural network controllers. Math. Probl. Eng. 1−9.